ELSEVIER

Thermochimica Acta 304/305 (1997) 229–237

thermochimica acta

Temperature calibration of temperature-modulated differential scanning calorimeters

A. Hensel, C. Schick*

Department of Physics, University of Rostock, Universitätsplatz 3, 18051 Rostock, Germany

Received 6 January 1997; accepted 23 April 1997

Abstract

Calibration of differential scanning calorimeters (DSC) is essential because it is not possible to calculate heat-flow rate and sample temperature directly from the quantities measured. The question arises whether the calibration used in the conventional DSC mode is also valid for temperature-modulated DSC (TMDSC). To prove this, a well-defined transition is needed which does not disturb the temperature profile within the sample during the modulation, the response of the whole system (calorimeter, sample, transition) must be linear. Some low-energy liquid-crystal transitions behave in this way under certain conditions and can be used for temperature calibration in TMDSC. The procedure is demonstrated for a smectic-A–nematic transition in a cyanobiphenyl liquid crystal (8OCB). Limitations of the method are discussed – in particular, rate effects. The TMDSC measurements also give some information about the order of phase transitions (8OCB: SN – second-order; NI – first-order). © 1997 Elsevier Science B.V.

Keywords: 8OCB; Complex heat capacity; DSC; Liquid crystal; Phase angle; Phase transition; Temperature calibration; Temperature-modulated DSC (TMDSC)

1. Introduction

Because of the design of the calorimeter cells used in differential scanning calorimetry and the unknown loss in any heat flow, it is not possible to calculate the heat-flow rate and the sample temperature directly from the measured temperature differences and temperatures, respectively [1,2], as is normally done in adiabatic and AC calorimetry. It is therefore necessary to calibrate the measured heat flow rate and the corresponding sample temperature. This is valid not only for DSC but also for temperature-modulated DSC (TMDSC) measurements. In TMDSC an additional third quantity needs calibration, namely the phase angle between heat-flow rate and heating rate signals and preliminary results for this correction in the glass-transition region are described in Ref. [3].

For conventional DSC there are well-developed calibration procedures for heat-flow rate and sample temperature [4–7]. It is unclear whether or not these procedures are directly applicable to TMDSC calibration. The first successful approaches for heat-flow rate calibration of TMDSC by using the same procedures as for DSC have been given [8–10]. In this paper, we shall focus on temperature calibration.

Temperature calibration in conventional DSC means the calibration of the thermometer used taking into account the thermal lag between thermometer and

*Corresponding author.

PII S0040-6031(97)00186-X

sample due to heat transfer [5–7]. To correct for thermal lag, the calorimeter should be calibrated at zero heating rate and the temperature of the effect under investigation should also be extrapolated to zero heating rate. This procedure, recommended by GEFTA [5], results in reproducible calibration independently of the type of DSC. For everyday use, the heating-rate dependence of the measured temperature must be considered. In the case of TMDSC, we must take into account not only the effect of the underlying heating rate q_0 but also possible influences of temperature amplitude and frequency and possible errors arising from the extensive numerical calculations and smoothing procedures used in the TMDSC data treatment. It is essential to calibrate the temperature scale for the different quantities after evaluation of the measured data from a TMDSC experiment, because there may be a shift between the temperature scale of the raw data and that after evaluation.

Temperature-modulated differential scanning calorimetry (TMDSC) [11–13] is an extension of conventional DSC. A temperature oscillation is superimposed on the linear heating or cooling rate (see Refs. [3,14,15] in this issue):

$$T(t) = T_0 + q_0 t + \sum_{n=1}^{\infty} (T_{a_n} \sin(n\omega t)) \qquad (1)$$

where t is time, T_0 the initial temperature, q_0 the constant underlying heating or cooling rate (henceforth, generally referred to simply as heating rate), T_{a_n} is the temperature modulation amplitude of the nth harmonic and $\omega = 2\pi/t_p$ is the angular frequency with t_p the modulation period.

The oscillating heating rate $q = dT/dt$ with heating-rate modulation amplitude $q_{a_n} = n\omega T_{a_n}$ results in a modulated heat-flow rate containing the response to the underlying heating rate q_0 and to the oscillations with the same harmonics as in the temperature signal. From this measured heat-flow rate different quantities can be determined. Gliding average of the heat-flow rate over one period yields the so-called total heat-flow rate, $\Phi_{total} = q_0 C_{p\,total}$, comparable with that of a conventional DSC measurement at the same heating rate q_0 [12,16,17]. Subtracting this averaged heat-flow rate from the measured one results in the so-called dynamic component. From this, the amplitude Φ_{a_1} of the first harmonic and the phase angle between heat-flow and heating rates can be determined by Fourier analysis (see, e.g. [13,16–21]). As a result, the signal-to-noise ratio may be significantly increased, which is one of the advantages of modulated techniques.

As pointed out by several authors in this issue, the heat capacity C_p^* can be considered to be a complex quantity [22–25] and the modulus $|C_p^*|$ can be obtained from

$$|C_p^*| = \frac{\Phi_{a_1}}{q_{a_1}} \qquad (2)$$

Other quantities can be calculated from $|C_p^*|$ and the phase shift between heat-flow and heating rates, e.g. the real and imaginary part of $C_p^* = C_p' - iC_p''$ [16,19], the reversing component which equals $|C_p^*|$ and the non-reversing component which equals $C_{p\,total} - |C_p^*|$ [17,18]. Calculations are only valid if the response to the first harmonic of the perturbation (temperature change) is included only in the first harmonic of the heat-flow rate amplitude (linear response). Otherwise, if a part of the response is found in higher harmonics, there are non-linear distortions of the signal (non-linear response).

It is well known that the response of a DSC is not always linear [26]. This is especially true for sample reactions with non-linear temperature responses, e.g. narrow phase transitions during which the sample temperature remains stationary for the time which the DSC needs for heat exchange processes. From a theoretical description of the DSC, we can derive rules to get correct values, e.g. of melting temperatures [1,2,27–31]. The most common result gives a construction for the 'peak onset temperature' which is a kind of measuring parameter, independently indicating first-order transition temperatures of pure compounds. This construction is the basis of temperature calibration in conventional DSC using materials with well-defined first-order phase transitions [5,6].

Because of the Fourier analysis used in the TMDSC evaluation technique, it is not so easy to correct for a possibly non-linear response of the calorimeter. The 'peak onset temperature' becomes meaningless as the prerequisites for the construction procedure are not fulfilled in TMDSC: there is no linearly increasing heat transfer into the sample (which remains at constant temperature during the transition) resulting from the linearly increasing oven temperature as with normal DSC. In TMDSC, we have to choose a

phase transition for temperature calibration which gives a linear response all over the transition range.

The question now arises: how to check the linearity of the whole system? This means the calorimeter itself as well as the sample and the specific transition are involved. Wunderlich [32] considers a DSC system to be linear if it can be described by linear differential equations [33], but this definition is not very helpful for testing the linearity of the apparatus – including the sample in the transition region – because of the unknown boundary conditions. We have to consider, say e.g., the time dependence of the sample temperature. Does it remain constant as is the case for first-order transitions, or does it follow the modulation in a certain way? Because it is very difficult to prove linearity of a measurement during a phase transition in this way, we prefer another definition of linearity which is directly related to the measuring process. From a mathematical point of view linearity is defined as follows [34]

$$f(ax) = af(x) \tag{3a}$$

$$f(x+y) = f(x) + f(y) \tag{3b}$$

where x and y represent the perturbation (i. e. the temperature), $f(x)$, $f(y)$ and $f(x+y)$ the respective responses of the system (i.e. the heat flow) and a an element of rational numbers. In our case, these quantities are scalars and both equations are equivalent for checking the linearity of the system. We used Eq. (3a), which means that an increase of the perturbation results in an increase of the response by the same factor. In TMDSC, we can change the perturbation by varying the modulation amplitude as well as the sample mass. In conventional DSC, it is possible to use different sample masses or heating rates to change the perturbation.

Non-linear behaviour, in the temperature range of the phase transition, depends not only on the magnitude of heat-flow rates but also on the nature of the phase transition. As shown by Ozawa [26] and in Fig. 1, Eq. (3a) does not even hold for the melting of sub-milligram amounts of indium. The DSC response – the measured heat-flow rate – of the melting of 0.48 mg indium does not equal the fourfold signal of a 0.12 mg sample. The reason is that during a first-order phase transition the sample temperature

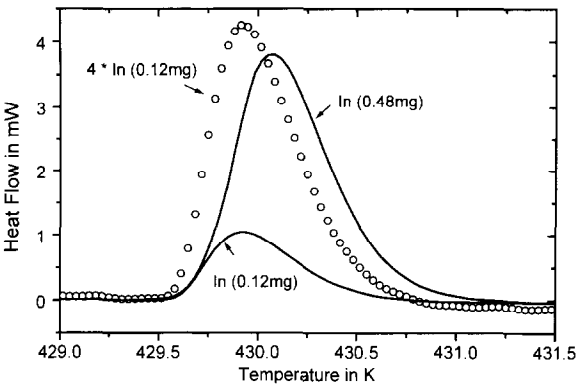

Fig. 1. DSC curve of indium melting with two different masses at $q = 10$ K/min, $m_p = 0.12$ mg and 0.48 mg. ○ – the 0.12 mg indium curve multiplied by 4.

remains constant, independently of the temperature programme. The measured heat-flow rate is only determined by the heat flow paths, depending on the design of the calorimeter. From AC calorimetric studies, it is known that this yields an additional phase angle [35,36]. Such transitions are not suitable for temperature calibration of TMDSC.

We need a phase transition which follows the modulation and leads to linear behaviour for the whole system. This should be a second-order transition. From previous studies on temperature calibration on cooling, it is known that some of the liquid-crystal phase transitions do not supercool [37–39] and there are other papers in this issue which show that some liquid-crystal transitions are of second order [35,36]. For example, the smectic-A–nematic transition (SN) of 4.4′-*n*-octyloxycyanobiphenyl (8OCB) [40] shows no supercooling, whereas from measurements at very slow scan rates it is found that this transition has a natural width of ca. 0.5 K [39]. We have therefore checked the SN transition of 8OCB for linear behaviour and for possible use for temperature calibration in TMDSC.

2. Apparatus and material

The phase behaviour of 8OCB was investigated in heating and cooling using Perkin–Elmer DSC-7 and Setaram DSC-121. Both calorimeters were used in the

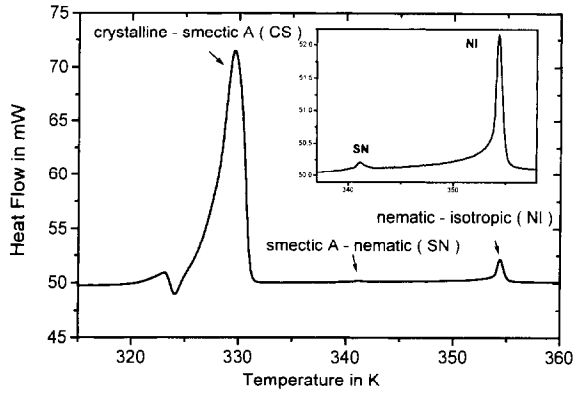

Fig. 2. Uncorrected DSC curve on heating of 4.4′-octyloxycyanobiphenyl (8OCB): $q = 10$ K/min, and $m_p = 4$ mg.

conventional (DSC) as well as in temperature-modulated (TMDSC) mode. All evaluations, namely calculation of $|C_p^*|$ and of phase angle, was performed with self-made software. Fig. 2 shows a typical DSC trace including the crystal–smectic A (CS), smectic-A–nematic (SN) and nematic–isotropic (NI) transitions of 8OCB. The compound was used as received from MERCK [40].

The temperature scale of the calorimeter was calibrated in the conventional DSC mode, as usual with indium and lead at a heating rate of 10 K/min. The heat-flow rate calibrant was sapphire. The purge gas was nitrogen at a flow rate of 1 l/h. The temperature of the calorimeter block of the Perkin–Elmer DSC-7 and the room temperature were kept well stabilised at (-75 ± 0.1) and (27 ± 0.5)°C, respectively, in order to realise reproducible scans. The scanning rate for the DSC experiments was 10 K/min, if not shown otherwise. TMDSC experiments were performed with sawtooth modulation using the Perkin–Elmer DDSC software or by setting up the corresponding programme with the standard temperature/time programming module from Setaram. From the dynamic part of the heat-flow rate, the modulus of complex heat capacity, according to Eq. (2), and the phase angle were determined using the same self-made evaluation software for both calorimeters (the built-in Perkin–Elmer software yields the same result). The modulation parameters and the underlying heating rate were varied over a wide range to observe their influence on the transition. To study transitions close to equilibrium, modulated measurements were performed in the quasi-isothermal mode using the Setaram DSC-121.

In the following, we focus on the smectic A nematic transition of 8OCB. The peak maximum temperature of the transition was used as measured, further corrections [41] would have little effect because of the very small peak height, 0.1 mW for the 4 mg sample, which corresponds to a peak in specific heat capacity of 0.15 J/gK.

3. Proof of linearity

The linearity of the SN transition for 8OCB, in both normal DSC and TMDSC, was investigated by observing the effects of experimental parameters on the final signals. In conventional DSC, 4 mg and 12 mg samples gave c_p curves that were identical within experimental error (curve 1, Fig. 3) showing that Eq. (3a) holds in marked contrast with the melting of indium (Fig. 1) and other first-order transitions. (To allow direct comparison of different experiments, all

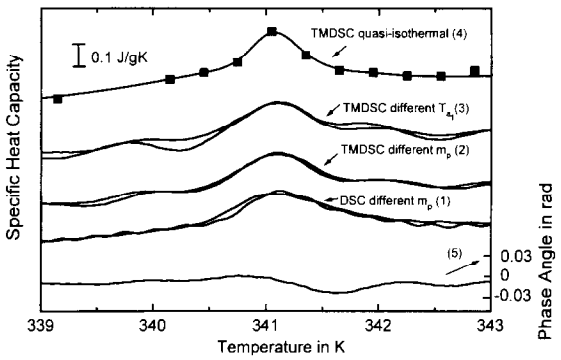

Fig. 3. Specific heat capacity c_p from conventional DSC and $|C_p^*|$ from TMDSC measurements on 8OCB in the smectic-A–nematic transition region. (1) – DSC measurements (PE DSC-7) at $q = 10$ K/min and different sample masses ($m_p = 4$ and 12 mg). (2) – TMDSC measurements (PE DSC-7) with $T_{a_1} = 0.2$ K, $t_p = 60$ s, $q_0 = 0.4$ K/min and different sample masses ($m_p = 4$ and 12 mg). (3) – TMDSC measurements (PE DSC-7) with $t_p = 60$ s and $q_0 = 0.4$ K/min ($m_p = 4$ mg and different modulation amplitudes, $T_{a_1} = 0.1$ and 0.2 K. (4) – Quasi-isothermal TMDSC measurements (Setaram DSC-121) with $T_{a_1} = 0.1$ K, $t_p = 600$ s, $q_0 = 0$, and $m_p = 21$ mg. (5) – Phase angle from a TMDSC measurement (PE DSC-7) with $T_{a_1} = 0.2$ K, $t_p = 60$ s, $q_0 = 0.4$ K/min, or j, see other figures and $m_p = 12$ mg.

heat-flow rate curves have been normalised to specific heat capacity $c_p = \Phi/m_p^* q_0$ where m_p is sample mass.) The same samples were also used to check the influence of mass on $|C_p^*|$ from TMDSC. For the conditions given for curve 2 in Fig. 3, it is clear that the two masses again gave the same curve. Identical curves were also obtained when the mass (4 mg) was held constant but the amplitude of modulation was doubled – curve 3 in Fig. 3.

As the peak area of ca. 0.08 J/g is nearly the same for DSC and TMDSC measurements, it seems that there is no latent heat involved in this smectic-A–nematic transition. To study the heat capacity anomaly around the transition, we made quasi-isothermal experiments with the Setaram DSC 121. A 21 mg sample was heated to the required measuring temperature and annealed for 30 min to reach equilibrium. The average value of $|c_p^*|$ from 10 periods is plotted in Fig. 3, curve 4. From the measured values, a transition peak with a half width of ca. 0.5 K and a peak height of ca. 0.15 J/g K is found to be in good agreement with the results from both conventional DSC and TMDSC measurements. As shown in curve 5, there is no significant change in phase angle during the SN transition. The heat capacity anomaly as well as the absence of supercooling [39] and any change in phase angle indicates that the smectic-A–nematic transition of 8OCB is of the second order [35,36].

Similar measurements were also performed at the nematic–isotropic (NI) transition of 8OCB. Fig. 4 shows that for normal DSC linearity only holds for

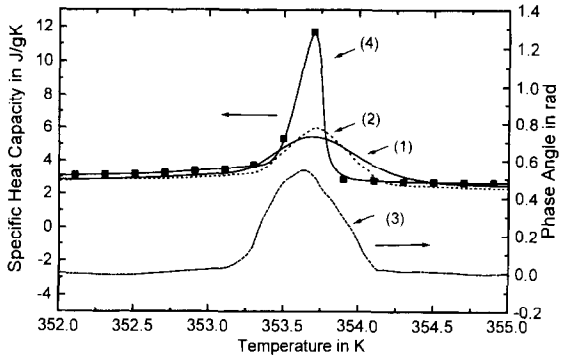

Fig. 5. Specific heat capacity c_p from DSC and $|C_p^*|$ from TMDSC measurements on 8OCB in the nematic–isotropic transition region. (1) – DSC measurements (PE DSC-7) at $q = 10$ K/min and $m_p = 4$ mg. (2) – TMDSC measurements (PE DSC-7) with $T_{a_1} = 0.2$ K, $t_p = 60$ s, $q_0 = 0.4$ K/min, and $m_p = 4$ mg. (3) – Phase angle between heat-flow rate and heating rate. Measuring conditions same as for curve 2. (4) Quasi-isothermal TMDSC measurements (Setaram DSC-121) with $q_0 = 0$, $T_{a_1} = 0.1$ K, $t_p = 600$ s, and $m_p = 21$ mg.

small sample masses. Results for scanning and quasi-isothermal TMDSC measurements are plotted in Fig. 5. The curves from the DSC and the TMDSC scans are similar but not in such a good agreement as for the SN transition. The peak in the $|c_p^*|$-curve seems to be narrower, although a much higher peak results from the quasi-isothermal measurements. The reason for this can be seen from the original heat-flow rate vs. time plot (Fig. 6). During the heating part of the temperature modulation of $\Delta T = 0.6$ K an endother-

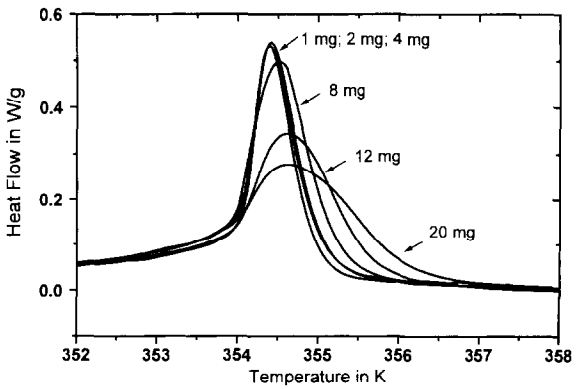

Fig. 4. Normalised heat-flow rate DSC curves for 8OCB in the nematic–isotropic transition region (PE DSC-7) with $q = 10$ K/min for different sample masses.

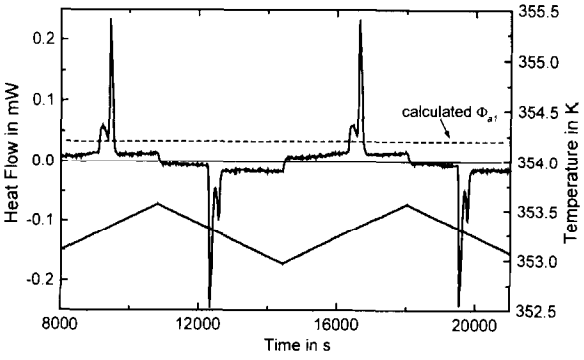

Fig. 6. Part of the measured heat-flow rate (endothermic upwards) from a TMDSC experiment (Setaram DSC-121) in the nematic–isotropic transition region ($q_0 = 0$, $T_{a_1} = 0.3$ K, $t_p = 7200$ s, $m_p = 21$ mg – the local heating rate is 0.01 K/min.).

mic double peak is observed and there are corresponding exothermic peaks in cooling. The peak area of these peaks (2.5 J/g) is in agreement with that determined from the conventional DSC scan at $q = 10$ K/min (2.4 J/g) but not with that of the quasi-isothermal TMDSC measurement (see curve 4, Fig. 5). From the steady-state values before and behind the peak, the heat-flow rate amplitude is ca. 0.015 mW which is in agreement with the values outside the transition. However, the Fourier analysis gives a figure of ca. 0.033 mW, as indicated by the dashed line in Fig. 6. This high value causes the very high peak in $|c_p^*|$ in Fig. 5 (curve 4). Because of the different position of the peaks – which dominate the first harmonic – relative to the temperature signal with increasing temperature during a scan, a drastic change in phase angle (curve 3, Fig. 5) can be observed. It can be seen from Figs. 4 and 5 that these curves are dependent on measuring conditions, in other words, linearity does not hold for this transition. The NI transition of 8OCB seems to be of the first order. The same behaviour – a second-order SN and weak first-order NI transition – was found for 8CB [35], the *n*-octyl analogue of the present (8OCB) material.

From these results it can be seen that there are transitions at well-defined temperatures which follow the temperature modulation without supercooling and result in a linear behaviour of the entire measuring and data treatment system. The smectic-A–nematic transition of 8OCB can therefore be used to investigate the influence of different measuring conditions on temperature calibration for TMDSC.

4. Influence of measurement conditions on temperature calibration

In TMDSC parameters such as temperature amplitude, the modulation period, underlying heating rate, sample mass, purge gas, etc. can be chosen over a rather wide range. In the following, we will discuss how temperature calibration in TMDSC is influenced by the first three of these parameters.

The temperature amplitude was varied between 0.07 and 3.4 K, fixing all the other parameters as given in the legend of Fig. 7. As a result the peak temperature was not affected, if temperature amplitudes were smaller than 2 K, but there was considerable peak broadening which can be seen from the decreasing peak height for temperature amplitudes higher than 0.2 K. An amplitude of $T_{a_1} = 0.2$ K equals a peak-to-peak temperature difference of ca. 0.4 K, the same order of magnitude as the peak width of ca. 0.5 μK. That means the peak becomes significantly wider if the temperature modulation passes most of the transition during one heating or cooling cycle. In other words, the temperature resolution of TMDSC measurements is given by the temperature amplitude chosen. The temperature amplitudes of more than 1 μK, that are often used, seem to be too high; they result in a loss of accuracy.

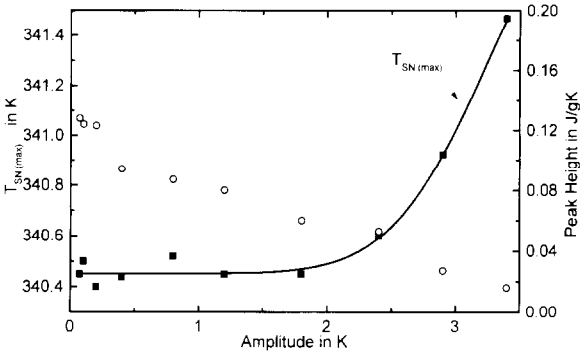

Fig. 7. ■ – Peak temperature $T_{SN\ (max)}$ and ○ – peak height of the smectic-A–nematic transition of 8OCB as a function of modulation amplitude T_{a_1} (PE DSC-7, $0.07 \leq T_{a_1} \leq 3.4$ K, $t_p = 50$ s, $q_0 = 0.4$ K/min, $m_p = 12$ mg).

To study the effect of modulation period, this was varied over the (12–300) s range, keeping the other parameters fixed as shown in Fig. 8. As a result, the peak temperature is not significantly influenced for periods shorter than 200 s, but for periods longer than ≈60 s the peak becomes broader and shallower. Due to the underlying heating rate of $q_0 = 0.4$ K/min, nearly the whole peak is passed within one period for periods longer than 60 s. Therefore, for longer periods the well-known prerequisite for accurate TMDSC measurements – to perform at least some modulations during the effect under investigation – is not satisfied and results in a loss of information.

The influence of the underlying heating rate can be studied for both conventional DSC and TMDSC. The measurements were therefore made in both these modes. The rate-dependent standard calibration procedure in conventional DSC was checked with indium.

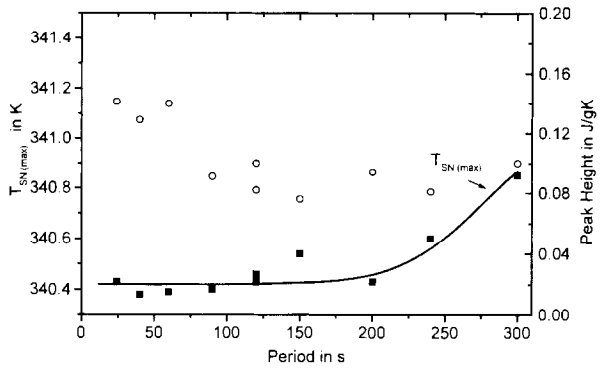

Fig. 8. ■ – Peak temperature $T_{SN\,(max)}$ and ○ – peak height of the smectic-A–nematic transition of 8OCB as a function of modulation period t_p (PE DSC-7, 12 s$\leq t_p \leq$300 s, $T_{a_1} = 0.2$ K, $q_0 = 0.4$ K/min, $m_p = 12$ mg).

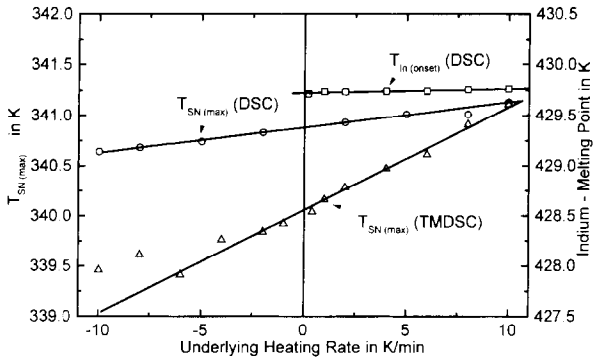

Fig. 9. Heating-rate dependence of transition temperatures for DSC and TMDSC measurements (PE DSC-7). □ – DSC $T_{In\,(onset)}$ indium, $m_p = 0.8$ mg; ○ – DSC $T_{SN\,(max)}$ 8OCB smectic-A–nematic, $m_p = 4$ mg; Δ - TMDSC $T_{SN\,(max)}$ 8OCB smectic-A–nematic, ($0.1 \leq T_{a_1} \leq 0.25$ K, $t_p = 12$ s, $m_p = 4$ mg).

The instrument had been calibrated in the usual way with indium and lead for a heating rate of 10 K/min. Fig. 9 shows that the indium peak onset temperature was unaffected by the heating rate. This was because of automatic thermal lag compensation [42] which could not be switched off in our equipment. Due to supercooling, the corresponding measurements were not possible in the cooling mode. For the peak temperature of the smectic-A–nematic transition of 8OCB a slightly different behaviour can be observed. The increased slope relative to indium is caused by different thermal conductivities between pan and sample and within the sample itself for both substances: the indium is in the solid while the 8OCB is in the liquid state before the transition. These differences are not included in the automatic thermal lag compensation. Temperature calibration could also be carried out in the cooling mode [39] because no supercooling can be observed for this transition.

The TMDSC measurements show (Fig. 9) a significantly larger slope for the rate dependence of the SN transition. The slope of about 0.08 K/(K/min) is in good agreement with typical results for the thermal lag of the Perkin–Elmer measuring system as determined without any thermal lag compensation [4,27].

5. Conclusions

Temperature calibration of temperature-modulated DSC can be performed with special second-order phase transitions. Because Fourier analysis is used for the calculation of different quantities in TMDSC, it is essential to show that linear behaviour holds for the whole measuring system, including the transition itself. Proof can be obtained from a study of the effects of sample mass or temperature amplitude. The smectic-A–nematic transition of 8OCB gives linearity for small temperature amplitudes ($T_{a_1} \leq 0.2$ K) because of the relatively small width (0.5 K) of this transition. Generally, such a transition can be used both for temperature calibration in TMDSC and for studying the influence of different measuring conditions on temperature calibration.

As shown in Figs. 7 and 8, temperature calibration of the Perkin–Elmer DSC-7 is independent of temperature amplitude and modulation period over relatively wide ranges. The most important parameter for precise temperature calibration is the underlying heating rate, see Fig. 9. DSCs are often calibrated for heating rates of 10 or 20 K/min. For TMDSC, the underlying heating rate must be drastically reduced to obtain reasonable results. Depending on the apparatus, the difference between heating rate used for conventional temperature calibration and that used for TMDSC measurements may shift the temperature scale by a few degrees and must always be taken into account (Fig. 9). Some additional problems occur if there is a software correction for thermal lag effects in DSC mode. This must be switched off as done automatically by the Perkin–Elmer software in the DDSC

mode or manually for Setaram calorimeters. If one wants to use the conventional DSC mode temperature calibration in TMDSC measurements, we recommend calibration according to GEFTA [5] with extrapolation to zero heating rate. Then, with or without software correction for rate effects, the possible uncertainties in temperature calibration near zero heating rate, as recommended for TMDSC measurements, are relatively small. For heating rates smaller than 1 K/min the deviations are less than 0.2 K and this is within the experimental error. For temperature calibration in TMDSC mode a second-order transition is necessary.

Results for the SN and the NI transitions of 8OCB show that, in TMDSC as in AC calorimetry [35,36], the measured response to a temperature perturbation in a phase transition region depends strongly on the type of transition (first or second order) under investigation. This is a very important result for studying, for example, the melting of polymers or other broad transitions where it raises the possibility of determining the order of the transition in question. In every case, the linearity of the system must be proved before interpretation of the results. Otherwise calculated quantities like reversing or real and imaginary parts of heat capacity may be influenced by non-linear distortions. Thus calculation of the imaginary part of the heat capacity according to $C_p'' = |C_p^*|\sin(\delta)$ in the nematic–isotropic transition region from the observed peak in phase angle (see Fig. 5) would give a meaningless quantity because the peak in phase shift in this case is caused by heat-transfer effects and not related to any time-dependent (or complex) heat capacity [3].

Acknowledgements

The authors gratefully acknowledge many interesting and clarifying discussions with G.W.H. Höhne, M. Richardson and B. Wunderlich. A. Hensel thanks the government of Mecklenburg-Vorpommern for financial support.

References

[1] B. Wunderlich, Thermal Analysis, Academic Press, New York, 1990.
[2] W. Hemminger, and G. Höhne, Calorimetry, Verlag Chemie, Weinheim, 1984.
[3] S. Weyer, A. Hensel and C. Schick, this issue.
[4] G.W.H. Höhne, H.K. Cammenga, W. Eysel, E. Gmelin and W. Hemminger, Thermochim. Acta, 160 (1990) 1.
[5] S. M. Sarge, W. Hemminger, E. Gmelin, G. W. H. Höhne, H. Cammenga and W. Eysel, J. Thermal Anal., 49 (1997), in press..
[6] M.J. Richardson and N.G. Savill, Thermochim. Acta, 12 (1975) 213.
[7] M. J. Richardson, The application of differential scanning calorimetry to the measurement of specific heat, in K. D. Maglic, A. Cezairliyan, V. E. Pelewtsky (Eds.), Compendium of Thermophysical Property Measurement Methods, Plenum Press, New York, 1992, Chap. 18, p. 519.
[8] A. Boller, Y. Jin and B. Wunderlich, J. Thermal Anal., 42 (1994) 307.
[9] G. van Assche, A. van Hemelrijck, H. Rahier and B. van Mele, this issue.
[10] B. Schenker, this issue.
[11] P.S. Gill, S.R. Saurbrunn and M. Reading, J. Thermal Anal., 40 (1993) 931.
[12] M. Reading, Trends Polym. Sci., 8 (1993) 248.
[13] M. Reading, B. K. Hahn, and B. S. Crowe, US Patent 5,224,775, 1993.
[14] J. M. Hutchinson and S. Montserrat, this issue.
[15] B. Wunderlich, A. Boller, I. Okazaki and K. Ishikiriyama, this issue.
[16] J.E.K. Schawe, Thermochim. Acta, 260 (1995) 1.
[17] B. Wunderlich, Y.M. Jin and A. Boller, Thermochim. Acta, 238 (1994) 277.
[18] M. Reading, A. Luget and R. Wilson, Thermochim. Acta, 238 (1994) 295.
[19] J.E.K. Schawe, Thermochim. Acta, 261 (1995) 183.
[20] J. E. K. Schawe and G. W. H. Höhne, Thermochim. Acta, in press.
[21] E. Gmelin, this issue.
[22] I. Alig, this issue.
[23] Y. H. Jeong, this issue.
[24] J. Korus, M. Beiner, K. Busse, S. Kahle and E. Donth, this issue.
[25] J. Schawe, this issue.
[26] T. Ozawa and K. Kanari, Thermochim. Acta, 253 (1995) 183.
[27] J. Schawe and C. Schick, Thermochim. Acta, 187 (1991) 335.
[28] G.W.H. Höhne and J.E.K. Schawe, Thermochim. Acta, 229 (1993) 27.
[29] J.E.K. Schawe, C. Schick and G.W.H. Höhne, Thermochim. Acta, 229 (1993) 37.
[30] J.E.K. Schawe, G.W.H. Höhne and C. Schick, Thermochim. Acta, 244 (1994) 33.
[31] J.E.K. Schawe, C. Schick and G.W.H. Höhne, Thermochim. Acta, 244 (1994) 49.
[32] B. Wunderlich, A. Boller, I. Okazaki and S. Kreitmeier, Thermochim. Acta, 282/283 (1996) 143.
[33] The Internal Dictionary of Applied Mathematics, Van Nostrand, Princeton, 1960.

[34] Elementary Linear Algebra, John Wiley and Sons., New York, 1994.
[35] D. Finotello, S. Qian and G. S. Iannacchione, this issue.
[36] M. Castro and J. A. Puertolas, this issue.
[37] J.D. Menczel and T.M. Leslie, Thermochim. Acta, 166 (1990) 309.
[38] J.D. Menczel and T.M. Leslie, J. Thermal Anal., 40 (1993) 957.
[39] G.W.H. Höhne, J. Schawe and C. Schick, Thermochim. Acta, 221 (1993) 129.
[40] Available as M24 from: Merck Ltd., Broom Road, Poole BH12 4NN, UK.
[41] K.H. Illers, Eur. Polym. J., 40 (1974) 911.
[42] Perkin–Elmer Thermal Analysis Newsletter 41, Perkin–Elmer Corp., Norwalk.